

Nano-indentation experiment for determining mechanical properties of typical cement phases at nano/micro-scale

Jia Fu^{1,2*}

¹ LGCGM, National Institute of Applied Sciences, 35708 Rennes, FRANCE

² Material Science and Engineering, Xi'an Shiyu University, 710065, Xi'an, CHINA

* Corresponding author's e-mail: fujia@xsyu.edu.cn

Abstract. Nano-indentation experiments are carried out on two cement pastes in order to get mechanical properties of cement pastes. For the comparison of initial cement paste, metakaolin as a valuable admixture for concrete/cement applications is added, considered to increase the reactivity of pozzolans. Statistical analysis on a number of indent points can be traced back to a medium modulus of elasticity. The averaged elastic moduli of typical phases in cement pastes are thus determined. Young's moduli of CH phases is about 44.7 GPa by nano-indentation experiment, which are close to the previous simulation values and other references. Besides, Young's moduli of Calcite and clinker averaged by nano-indentation experiment are 86.695 GPa and 102.230 GPa , which are separately in relative good agreement with simulation values of 84.549 GPa by Jia and $85.41\text{--}145.56\text{ GPa}$ (porosity: 10%) by Arar. A systematic approach is developed to validate and to assess the elastic parameters associated with each phase. The P-h curves of the simulation and experiment are compared to conclude on the feasibility of the methodology.

1. Introduction

In recent years, the Multi-Scale Modelling of Computational Concrete (MuMoCC) platform has been proposed and continuously improved^[1]. Multi-scale modeling of structural concrete performance is proposed^[2], and the different scales will be considered to reflect the atomic interaction^[3] and different length-scales^[4], and a unique constitutive behavior cannot be captured fully^[5] for the greater length-scale. There are mainly four regions of hydrated products, such as: voids region (the cumulative hydration voids), C-S-H region (including low density and high density), CH phase region and RC phases region (the residual cement in a cement paste).

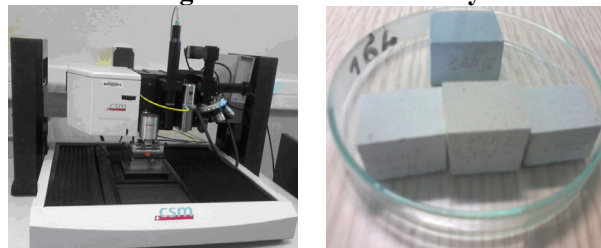
Nano-indentation can be used to understand differences in hydration products that result from water availability for clinker during hydration^[6]. Although its theoretical mechanism is very complex, the experimental measurements to calculate elastic modulus become the easiest way, mainly a variety of indentation experiments. The simulation results of CH^[7], calcite^[7], LD C-S-H^[8] and HD C-S-H^[8] have been studied previously. The nano-indentation experiment is used here to characterize other cement-based materials. Muller et al.^[9] has studied SEM BSE micrograph of different phases in ordinary Portland cement (OPC) paste at 7 days of hydration and point's position of the paste with $w/c=0.40$ after 28 days of hydration for the EDX-SEM analysis. Ulm and co-workers^[10,11] have provided the experimental techniques and analysis tools to provide a reliable, mechanical technical tools to identify the relative volume fractions and spatial distributions of cement hydration products in



cement paste samples produced with conventional cements. The average nanoscale material responses for each phases are the same for all portland cement pastes tested to date ^[12,13].

A large experimental nano-indentation campaign has been led to obtain a data basis of Young's modulus for the various phases of several cement pastes. These results may be used to validate the modeling approaches developed by the authors in previous publications. Although there are scientific reports on nano-indentation of cement pastes, however, these studies are almost based on statistical analysis ^[14] or molecular simulation ^[15], and its phase analysis at nano-scale has not yet been systematically studied. The results of the nano-indentation tests have been already published in reference of Fu et al. ^[6], this new paper presents the results for pastes with CEM I and Metakaolin. In this study, the indentation modulus and hardness will be discussed to obtain the experimental results in CH, LD and HD C-S-H phases thus to compare with the results of D. Keinde ^[16] and Constantinides ^[17]. As CH, C-S-H and clinker are main components in hydrated Portland cement paste, our task is to achieve the accuracy of the Young's modulus via nano-indentation experiment.

2. Nano-indentation experiment and regional indentation analysis



a) Nano-hardness platform b) Cement paste sample
Figure 1. CSM instrument and cement paste used in experiment.

The CSM instruments is used for the experiment, which includes: ultra nano-indentation tester head, nano-indentation tester head, atomic force microscopy and optical video microscope. Samples has the dimension of $1.1\text{cm} \times 1.1\text{cm} \times 1.1\text{cm}$. Parameters are the same with the published reference ^[6].

Composition and designation of the tested binder pastes are shown in Table 1.

Table 1. Composition and designation of the tested binder pastes

Composition (Kg/m ³)	CEMI	Limeston filler	Metakaolin	Water	Water/binder
B-CEM I	330	240	-	210	0.368
B-CEMI MK	280.5	240	49.5	210	0.368

Composition of the cements and mineral admixtures (limestone filler, metakaolin) are in Table 2.

Table 2. Composition and properties of cements and mineral admixtures

Components	CEMI (%)	Limeston filler (%)	Metakaolin (%)
CaO	64.53	-	0.1
CaCO ₃	-	96.8	-
SiO ₂	20.12	0.9	55
Al ₂ O ₃	5.03	-	40
Fe ₂ O ₃	3.12	-	1.4
MgO	0.98	-	0.2
K ₂ O	0.98	-	0.8
Na ₂ O	0.16	-	0.02
SO ₃	3.34	-	-
clinker content(%)	98	-	-
Specific surface (cm ² /g)	3649.9	4190	17000
Specific gravity (g/cm ³)	3.15	2.7	2.4

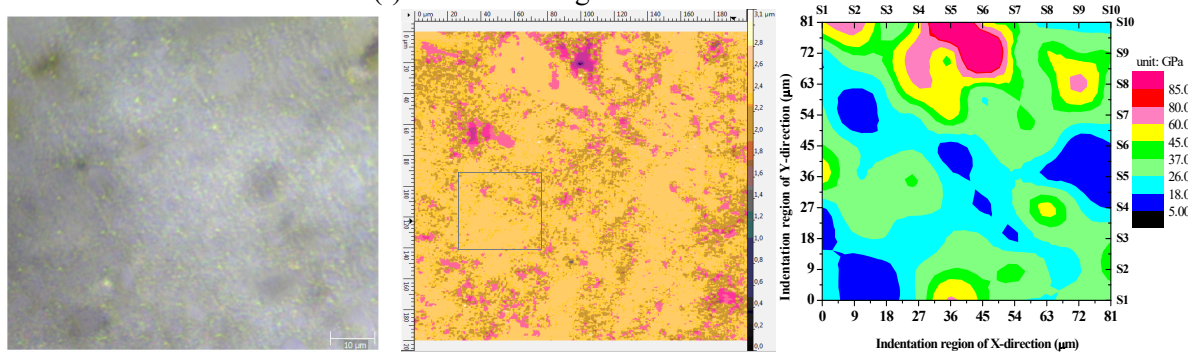
To highlight the different phases of samples, SEM analysis are made in the “Centre de Microscopie Electronique a Balayage et micro-Analyse (CMEBA)” in university of Rennes 1.

3. Results analysis and discussion

Nano-indentation experiment is carried out to determine elastic moduli of cement phases. Bountiful tests is applied to obtain mechanical properties of different phases [18]. Ulm and co-workers [19, 20] have studied hardened cement pastes using the technique of nano-indentation and related data analysis tools. It is generally believed that portland cement hydration products in hardness is not higher than 2GPa, and the elastic modulus is not higher than 45 GPa [17]. The reduced modulus is obtained and used. For obtaining Young's modulus, the assumption on the value of the Poisson ratio is required to transform from the reduced modulus to Young's modulus, which should be clearly precise.

3.1. Regional indentation analysis of B-CEM (I)

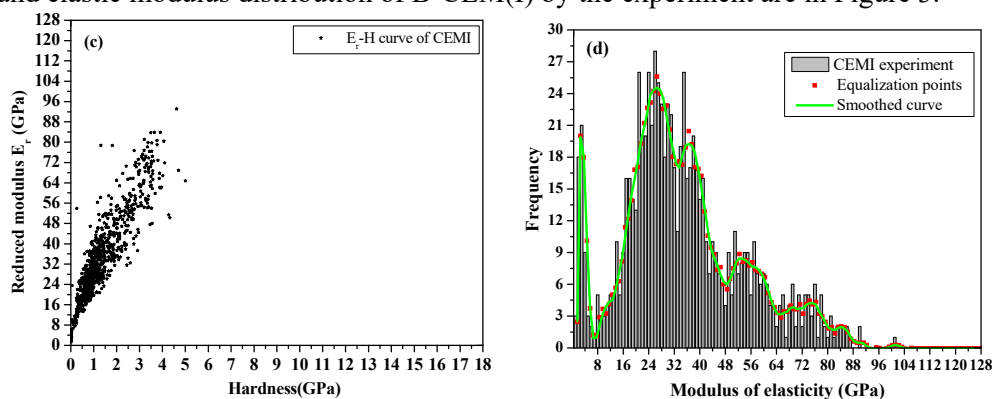
For B-CEM(I) sample, we focus on the analysis of hardness range of hydration products, the unhydrated particles will not be considered. Poisson coefficient is set to 0.2. Regional indentation of the B-CEM(I) matrix area (100 indents, $81 \times 81 \mu\text{m}^2$, indent distance $9 \mu\text{m}$, force 1.5mN) and elastic modulus distribution of B-CEM(I) is shown in Figure 2.



a) Indentation region b) Indentation area in the plane area c) The fitting areas of elastic modulus distribution
Figure 2. Elastic modulus distribution of B-CEM(I) by nano-indentation experiments

Figure 2 a) shows the 10×10 indents performed on the matrix. The marked plane area in Figure 2 b) is about $50 \text{nm} \times 50 \text{nm}$. The cement matrix region (the distance between two indents is $9 \mu\text{m}$) is assigned to the smoothed surface surrounded by the outlined indent area enclosed by the color lines. Figure 2 c) presents the fitting of the contour areas to show the possible surround areas by all data of the indentation points with contrast to Figure 2 a).

Meanwhile, the mapping matrices and E_r - H curves according to the experiment data can be used to analyse the main phases in the indentation area. The number of total indents on surface is 830. The E_r - H curve and elastic modulus distribution of B-CEM(I) by the experiment are in Figure 3.

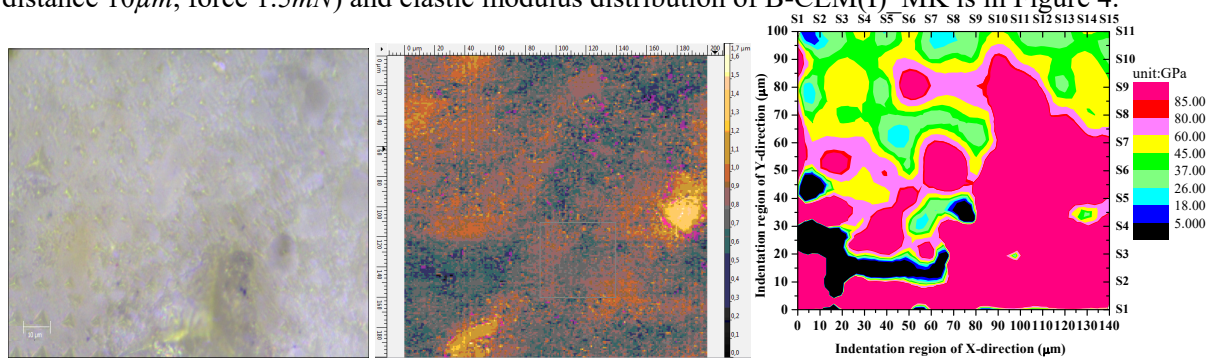


a) Distribution of the reduced modulus versus hardness b) Frequency histogram of elastic modulus
Figure 3. E_r - H curve and elastic modulus frequency histogram of B-CEM(I) sample

As is in Figure 3 a), the E_r - H curve basically turns to a kind of linear relationship. The averaged elastic modulus E_{HIT} of all the individual indents is about 35.746GPa and the averaged maximum depth h_{max} value is about 268.85nm . The evolution of the elastic modulus E_{HIT} and maximum depth h_{max} as a function of the indented position of the treated sample are recorded. Moreover, we can suppose from Figure 3 b) that elastic modulus of different phases are as follows: LD C-S-H is 26GPa , HD C-S-H is 36GPa , CH is $48\sim 52\text{GPa}$, Calcite is $64\sim 88\text{GPa}$.

3.2. Regional indentation analysis of B-CEM(I)_MK

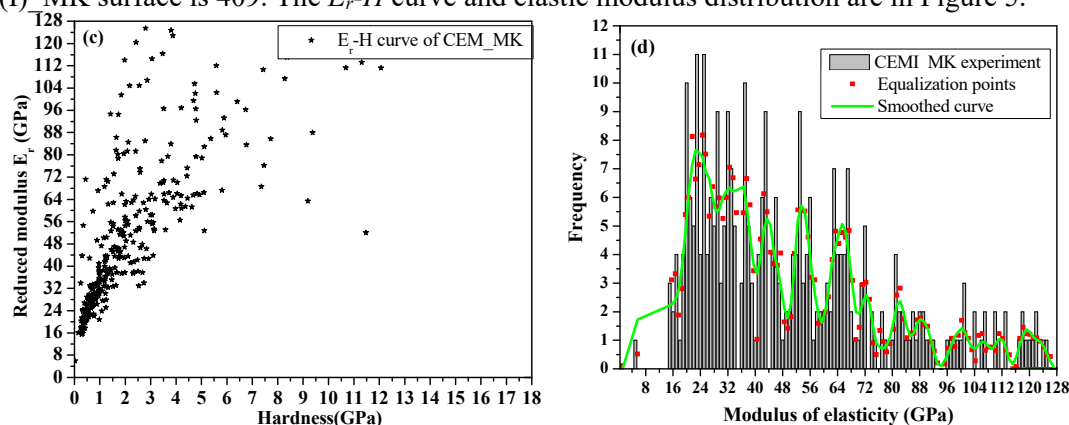
Similarly, during data processing of B-CEM(I)_MK sample, we focus on the analysis of hardness range of hydration products, the unhydrated particles will not be considered. The Poisson ratio value is set to 0.2. Regional indentation of the B-CEM(I)_MK matrix area (165 indents, $100\times 140\mu\text{m}^2$, indent distance $10\mu\text{m}$, force 1.5mN) and elastic modulus distribution of B-CEM(I)_MK is in Figure 4.



a) Indentation region b) Indentation area in the plane area c) The fitting areas of elastic modulus distribution
Figure 4. Elastic modulus distribution of B-CEM(I)_MK by nano-indentation experiments

Figure 4 a) shows the distribution of 15×11 indents performed on the matrix. The marked plane area in Figure 4 b) is about $50\text{nm}\times 50\text{nm}$. The indent distance is $10\mu\text{m}$ is assigned to the smoothed. Figure 4 c) presents the fitting of the contour areas to show the possible surround areas by all indent.

Meanwhile, the average of Young's moduli on the determined 165 indents enable to obtain an approximative mean value of the matrix modulus. Young's moduli on the determined indents enable to obtain an approximative mean value of the matrix modulus. The number of total indents on B-CEM(I)_MK surface is 409. The E_r - H curve and elastic modulus distribution are in Figure 5.



a) Distribution of the reduced modulus versus to hardness b) Frequency histogram of elastic modulus
Figure 5. E_r - H curve and elastic modulus frequency histogram of B-CEM(I)_MK sample

As is shown in Figure 5 a), the E_r - H curve basically turns to a kind of linear relationship. The averaged elastic modulus E_{HIT} of all the individual indents is about 57.240GPa and the averaged maximum depth h_{max} value is about 226.90nm . Moreover, we can suppose from Figure 5 b) that elastic

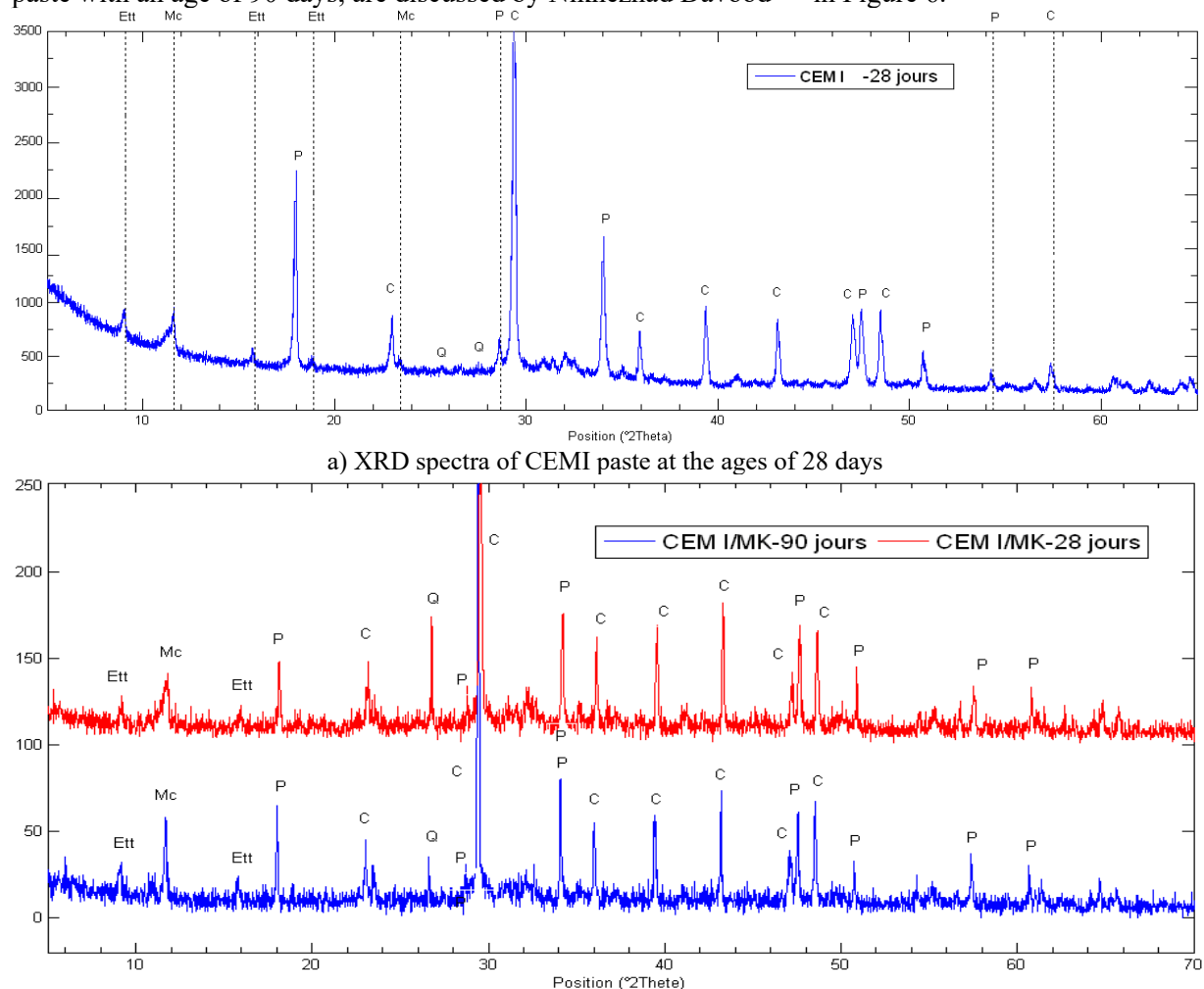
modulus of phases are as: LD C-S-H is 24GPa , HD C-S-H is 32GPa , CH and metakaolin hydration product is about $45\text{--}56\text{GPa}$, Calcite is $60\text{--}84\text{GPa}$, unhydrated clinker phase is about $96\text{--}124\text{GPa}$.

In a word, by comparison of the averaged elastic modulus E_{HT} , we can see that the elastic modulus of B-CEM(I)_MK on average is higher than the B-CEM(I), which shows that the addition of metakaolin can improve performance of cement matrix.

4. Analysis of indentation morphology, microstructures and elastic moduli

4.1. XRD spectra results of cement pastes

For various cement pastes, different phases can be observed by XRD spectra and determined according to their microstructures^[15]. X-ray experiments is proved to be effective, different pastes including B-CEM(I) and B-CEM(I)_MK by XRD spectra, with an age of 28 days and the CEMI_MK paste with an age of 90 days, are discussed by Niknezhad Davood^[21] in Figure 6.



b) Comparison of CEMI_MK paste at different ages of 28 days and 90 days
Figure 6. XRD spectra of the different pastes after 28 days and CEMI_MK after 90 days

Figure 6 shows the diffraction patterns on samples of binder pastes aged 28 days and 90. In Figure 6 a), a certain amount of calcite, portlandite, ettringite and monocarbonatealuminate are presented and characterized in pastes of CEMI and CEMI_MK. Besides, the quartz is also detected in CEMI_MK paste. Moreover, the peak of portlandite is much less intense for the pastes in which a low content of clinker is also predictable like CEMI_MK paste. Figure 6 b) shows the paste with metakaolin aged separately 28 days and 90 days, present the same minerals, where the monocarbonatealuminate peak is

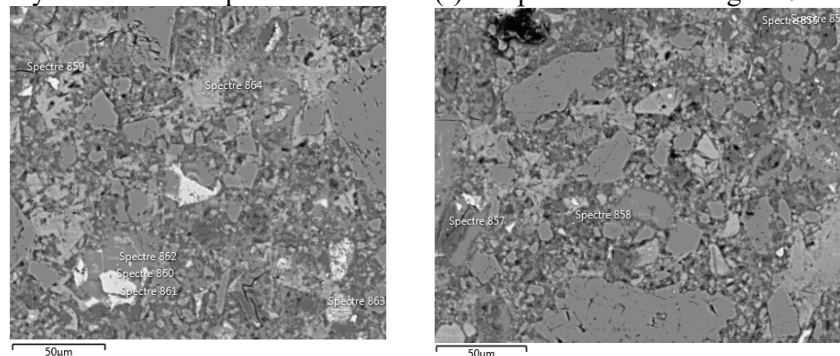
the strongest. Besides, for B-CEMI_MK sample, except for the there exist exceptional C-S-H pozzolanic. By Fig.6, there exists more CH in B-CEMI than in B-CEMI_MK and there exists more ettringite phases in B-CEMI_MK than in B-CEMI.

4.2. Indentation morphology and composition analysis

Following these indents by electron microscopy, we can confirm that most of these points are located in hydrated areas.

4.2.1 Composition analysis of feature points and microstructure of cement phases in B-CEM (I)

Composition analysis of different phases in B-CEM(I) sample is shown in Figure 7.



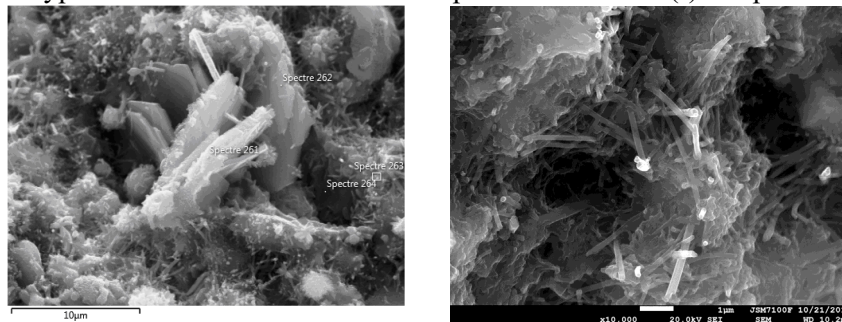
a) Composition analysis of area 1

b) Composition analysis of area 2

Figure 7. Composition analysis of different phases in B-CEM(I) sample

As in Figure 7, the corresponding composition tested points include the spectres of positions 859-864 in in Figure 7 a) and the spectres of positions 856-858 in Figure 7 b). Point 861 corresponds to limestone grain while point 860 corresponds to C3S grain and point 862 probably to inner C-S-H.

Figure 8 shows typical microstructures of different phases in B-CEM (I) sample.



a) The point 262 of CH and point 263 of C-S-H

b) The morphology of C-S-H

Figure 8. Image of typical microstructures in B-CEM (I) sample.

From Figure 8 a), the grown prismatic shape (needles like – SEM image at the right) is likely to be the ettringite phase. Besides, the lamellar test point 262 is possible on the CH phase. Meanwhile, the position of point 263 is probably to be the C-S-H phase as it is on the surface of the Cement particle. Moreover, the microcrystalline ettringite is verified in Figure 8 b), where the fibrous C-S-H coating on the cement particles is obvious, and C-S-H gel tends to be the perfect fibrous shape.

4.2.2 Composition analysis of feature points and microstructure of phases in B-CEM (I)_MK

Indentation morphology of different phases in B-CEM1_MK sample is in Figure 9.

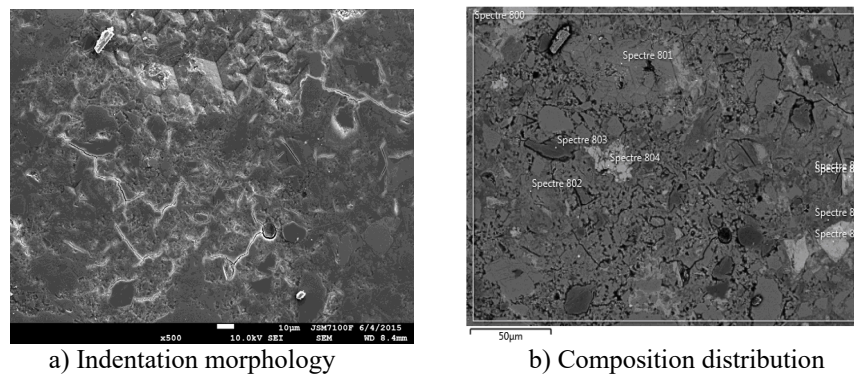
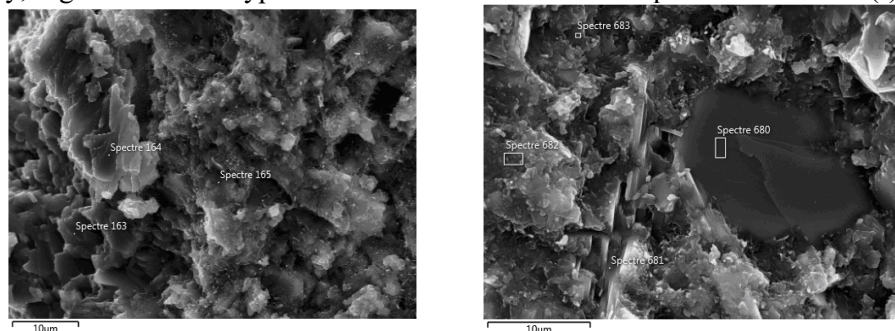


Figure 9. Indentation morphology and composition analysis of partial B-CEM(I)_MK sample

Figure 9 a) shows a partial indentation morphology, it can be seen that the different indent have different indentation depth. If the elastic modulus value is small, the indentation depth of the corresponding point is deeper. Figure 9 b) shows the corresponding composition points tested in the indentation morphology, it can be seen that, spectre 804 position in the white area may be C_2S phase. For the composition of different test points, the type and the percentage of each element in the tested point is given, thus the corresponding phase in each tested indentation point can be inferred. According to the chemical composition analysis and morphology analysis of these points, the results of the microscopic structure analysis matches to the analysis mentioned above.

Similarly, Figure 10 shows typical microstructures of different phases in B-CEM (I) MK sample.



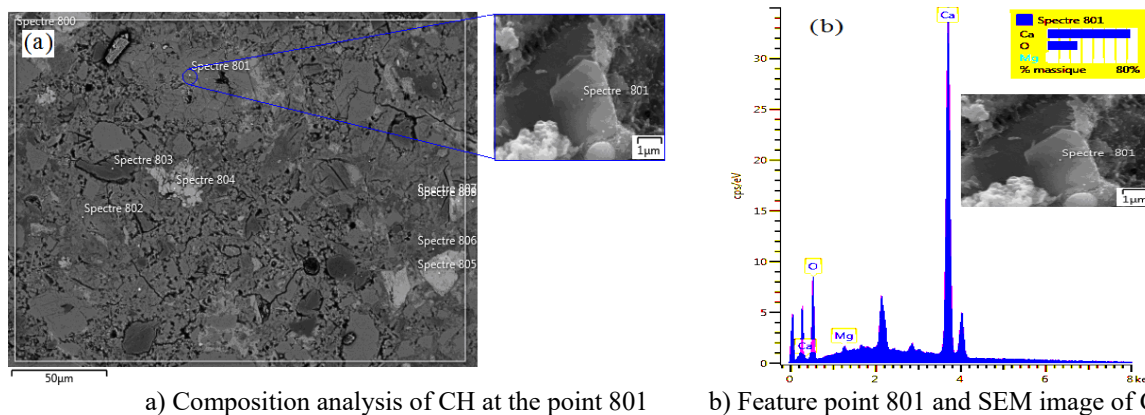
a) The test point 163 of CH b) The point 681 of CH and point 680 of limestone filler
Figure 10. Image of typical microstructures in B-CEM (I)_MK sample.

As can be seen from Figure 10, the test point 681 and the test point 163 with the sheet-like shape are possible to be CH phase, while the position of the test point 680 corresponds to limestone filler grain in Figure 10 b). Moreover, it is worth noticing that there are many composite products. The microscopic analysis results of these three points are all agreed with the chemical composition analysis.

In all, following these indents by electron microscopy, we can confirm that most of these points are located in hydrated areas. By the microstructure analysis of Figure 7- Figure 10, for B-CEMI and B-CEMI_MK, it can be estimated that there exist three types of microstructures: unhydrated products (C_3S , C_2S , C_3A and C_4AF), hydrated products (CH, LD CSH, HD CSH, ettringite and monocarboaluminate) as well as grain (limestone, calcite etc.).

4.3. Elastic moduli of cement phases by nano-indentation experiment

From the indentation morphology observation and composition analysis, CH phases is in Figure 11.

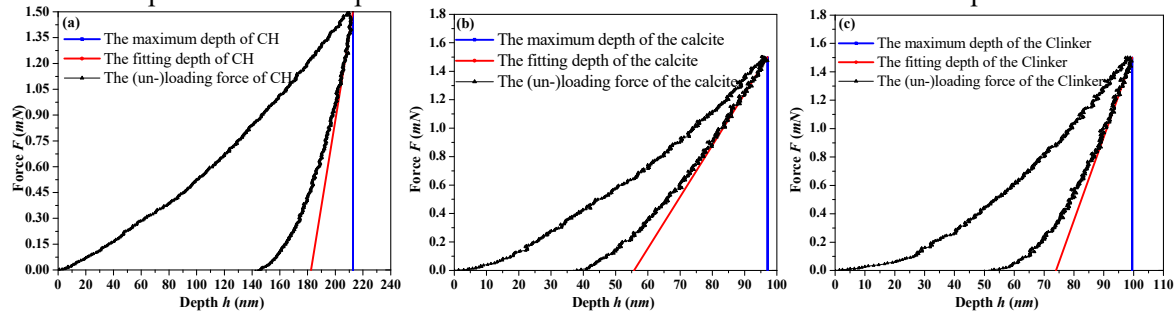


a) Composition analysis of CH at the point 801 b) Feature point 801 and SEM image of CH
Figure 11. Indentation morphology and composition analysis of CH

Figure 11 a) shows the chemical composition points tested, it can be seen that, spectre 801 position in the gray area is CH phase. Percentage of each element in point 801 in Figure 11 b) includes the mass element percentage (O 26.24%, Ca 73.38% and Mg 0.38%) and the atomic element percentage (O 47.03%, Ca 52.51%, Mg 0.45%), and the lamellar test point 801 is possible on CH phase.

The elastic moduli of LD C-S-H and HD C-S-H have been investigated^[6,8], according to the microstructure observed and confirmed, the indents of other phases under different samples are found and the corresponding P - h curves are pointed out. The representative P - h curves of CH, aggregate and clinker phases are averaged and determined, in Figure 12.

Figure 12 a) shows the representative experimental P - h curve of CH phase found in cement pastes, with corresponding elastic modulus is about 39.88 GPa, which is close to the simulation results of Jia et al.^[7] and Asroun et al.^[22]. Figure 12 b) and Figure 12 c) separately show the representative experimental curve of calcite and clinker phases with its corresponding elastic modulus of 86.695 GPa and 102.23 GPa are close to 84.549 GPa by Jia^[7]. and 85.41-145.56 GPa (porosity: 10%) by Arar^[23]. These results provide the basis parameters for multi-scale calculation on MuMoCC platform^[1,3].



a). Representative curve of CH b). Representative curve of calcite c). Representative curve of clinker
Figure 12. Representative experimental curves of aggregate and clinker phases

5. Conclusion

Nano-indentation experiments are carried out and regional indents are analyzed combined with the observation of morphology and analysis of the E_{HIT} frequency histogram. The experimental curves are analyzed and Young moduli are determined by the P - h curves. Conclusions are as follows:

1) By frequency histogram of elastic modulus E_{HIT} , four phase regions exist, of which the elastic modulus of unhydrated particles region is over 80 GPa, the elastic modulus of HD CS-H gel region is within the range of 32~36 GPa, CH region of 43~52 GPa and LD C-S-H gel region of 16~26 GPa.

2) Young's moduli of CH phases is about 44.7 ± 4.5 GPa by nano-indentation experiment, which is close to the result of CH 40.3 ± 4 GPa by Constantinides, 2004.

3) Young's moduli of Calcite and clinker averaged by nano-indentation experiment are 86.695 GPa and 102.230 GPa, which are separately in relative good agreement with simulation values of 84.549 GPa by Jia and 85.41-145.56 GPa (porosity: 10%) by Arar.

In all, these parameters provide evidence to obtain the mechanical properties of certain cement phases, thus to establish an accurate multi-scale model of concrete on MuMoCC platform.

Acknowledgments

The authors acknowledge the financial support provided by China Scholarship Council (CSC). Thanks to Qiufeng WANG for her proofreading. The authors are grateful for the assistance in SEM observations and EDS analysis of the staff of the CMEBA facility (ScanMAT, UMS 2001 CNRS University of Rennes 1) which received a financial support from the Région Bretagne and European Union (CPER-FEDER 2007-2014)

References

- [1] Kamali-Bernard S, Bernard F. (2009) Effect of tensile cracking on diffusivity of mortar: 3D numerical modelling [J]. *Computational Materials Science*, 47:178–185
- [2] Maekawa, K., Ishida, T., & Kishi, T., (2003) Multi-scale modeling of concrete performance[J]. *Journal of Advanced Concrete Technology*, 1(2): 91-126.
- [3] Bernard F, Kamali-Bernard S, Prince W., (2008) 3D multi-scale modelling of mechanical behaviour of sound and leached mortar [J]. *Cement and Concrete Research*, 38:449–458
- [4] J. Fish, (2006) Bridging the scales in nano engineering and science[J]. *Journal of Nanoparticle Research*, 8.
- [5] W.A. Curtin, R.E. Miller, (2003) Atomistic/continuum coupling in computational materials science [J]. *Modelling and Simulation in Materials Science and Engineering*. 11: 33-68.
- [6] Jia Fu, Siham Kamali-Bernard, Fabrice Bernard, Marilyne Cornen, (2018) Comparison of mechanical properties of C-S-H and Portlandite between nano-indentation experiments and a modelling approach using various simulation techniques, *Composite part B: Engineering*, 151: 127-138.
- [7] Jia Fu, Fabrice Bernard, Siham Kamali-Bernard, (2017) First-principles calculations of typical anisotropic cubic and hexagonal structures and homogenized moduli estimation based on the Y-parameter: Application to CaO, MgO, CH and Calcite CaCO_3 [J]. *Journal of Physics and Chemistry of Solids*, 101:74-89..
- [8] Jia Fu, Fabrice Bernard, Siham Kamali-Bernard, (2018) Assessment of the elastic properties of amorphous Calcium Silicates Hydrates (I) and (II) structures by Molecular Dynamics Simulation, *Molecular Simulation*. 44(4):285-299.
- [9] Muller Arnaud Charles Albert. (2014) Characterization of porosity & CSH in cement pastes by ^1H NMR. Thèse de doctorat. École Polytechnique Fédérale de Lausanne.
- [10] F-J Ulm, M. Vandamme, C. P. Bobko et al., (2007) Statistical indentation techniques for hydrated nanocomposites: concrete, bone, and shale[J]. *Journal of the American Ceramic Society*, 90(9): 2677-2692.
- [11] L. Sorelli, G. Constantinides, F-J Ulm et al. (2008) The nano-mechanical signature of ultra-high performance concrete by statistical nanoindentation[J]. *Cement and Concrete Research*, 38(12): 1447-1456.
- [12] M. Vandamme, (2008) The Nanogranular Origin of Concrete Creep: A Nanoindentation investigation of microstructure and fundamental properties of Calcium-Silicate-Hydrates, Ph.D. Thesis, Massachusetts Institute of Technology, Cambridge, MA.
- [13] V. Zanjani Zadeh, C.P. Bobko. (2014). Nano-mechanical properties of internally cured kenaf fiber reinforced concrete using nanoindentation[J]. *Cement and Concrete Composites*, 52, 9-17.
- [14] Ye, G. (2003). Experimental study and numerical simulation of the development of the microstructure and permeability of cementitious materials. TU Delft, Delft University of Technology.

- [15] Ye, G., Van Breugel, K., & Fraaij, A. L. A. (2003) Three-dimensional microstructure analysis of numerically simulated cementitious materials[J]. *Cement and Concrete Research*, 33(2), 215-222.
- [16] Keinde, D. (2014). Etude du béton à l'échelle mesoscopique: simulation numérique et tests de micro-indentation, Doctoral dissertation, INSA de Rennes.
- [17] Constantinides G. et al., (2004) The effect of two types of CSH on the elasticity of cement-based materials: Results from nanoindentation and micromechanical modeling[J]. *Cement and concrete research*, 34(1), 67-80.
- [18] Zanjani Zadeh Vahid, (2013) *Nanomechanics and Multiscale Modeling of Sustainable Concretes*. Ph.D. Thesis, North Carolina State University.
- [19] Constantinides, G., & Ulm, F. J., (2007) The nanogranular nature of C–S–H[J]. *Journal of the Mechanics and Physics of Solids*, 55(1), 64-90.
- [20] G.Constantinides, K.S.Ravi Chandran, F-J Ulm, et al., (2006) Grid indentation analysis of composite microstructure and mechanics: principles and validation[J]. *Materials Science and Engineering: A*, 430(1), 189-202.
- [21] Davood NIKNEZHAD. (2016). Contribution à l'étude du comportement mécanique, du retrait et des propriétés de transport des bétons autoplacants avec additions minérales, approche numérique et expérimentale, Doctoral dissertation, INSA de Rennes.
- [21] ASROUN Nasser, et al. (2013) Nanoindentation simulation of concrete with various indenter forms and yield strengths[J]. *International Journal of Civil & Structural Engineering*, 4(1): 36-45.
- [22] Arar, M. (2016). Elastic properties of cement phases using molecular dynamic simulation.[D] Doctoral Dissertation, Ryerson University.